

WALL CLUTTER MITIGATION FOR MIMO RADAR CONFIGURATIONS IN URBAN SENSING

Fauzia Ahmad and Moeness G. Amin

Radar Imaging Lab, Center for Advanced Communications, Villanova University,
Villanova, PA 19085, USA.

ABSTRACT

Strong front wall returns tend to obscure indoor targets and render through-the-wall target detection difficult and challenging. Among the various techniques proposed for wall clutter mitigation under monostatic radar operation is subspace projection. This technique uses the strength of the wall EM reflections relative to that of the target to separate the wall subspace from the target subspace. In this paper, we present analyses of the subspace projection approach for suppressing wall clutter and preserving indoor targets in multi-input multi-output (MIMO) through-the-wall radar imaging systems. We highlight the similarities and the differences in performance of the subspace technique under MIMO and monostatic configurations. Supporting results based on simulated and experimental data are provided.

1. INTRODUCTION

Sensing through obstacles such as walls, doors, and other visually opaque materials, using microwave signals is emerging as a powerful tool supporting a range of civilian and military applications [1]. Through-the-wall radar imaging (TWRI) has been recently sought out for surveillance and reconnaissance in urban environments, requiring not only behind-the-wall detection of humans and interior objects, but also the layout of the building. Additionally, this technology can also be used by fire fighters to detect and locate survivors, and in search and rescue missions in natural disasters.

Multiple input multiple output (MIMO) radar is an emerging technology with a rising interest in the radar community. By emitting orthogonal waveforms from the transmit array antennas and utilizing matched filter banks in the receivers to extract the orthogonal waveform components, MIMO radar systems can exploit the spatial diversity and the higher number of degrees of freedom to improve resolution, clutter mitigation, and target classification. In particular, a collocated MIMO radar can provide effective array designs to achieve an extended virtual array, which is the sum coarray of the transmit

This work was supported by ONR under grant N0014-10-1-0455.

and the receive arrays [2]. A distributed MIMO radar, on the other hand, is capable of jointly estimating the Direction-of-Departure (DOD) and Direction-of-Arrival (DOA) of targets for enhanced target localization.

The application of MIMO configurations in TWRI has been recently explored in [3], [4]. In both references, however, a moving target assumption is made so as to remove clutter by change detection techniques wherein consecutive radar images are acquired and subtracted. For many scenarios, the scenes are stationary and the targets of interest do not exhibit translational or oscillatory movements. In these cases, front wall clutter, which often obscures targets, should be removed prior to imaging. Effective suppression of the front wall reflections allows target detection and classification.

There exist several techniques to remove wall clutter for monostatic array configurations [5]-[7]. Among these techniques is the subspace projection method in which the strength of the wall EM reflections relative to that of the target is used to separate the wall subspace from the target subspace [6]. The two subspaces are obtained using singular value decomposition (SVD) of the observation matrix, whose columns, for stepped-frequency operation, are the frequency measurements at the different antennas. The properties exhibited by the wall reflections under the monostatic configuration change when considering a MIMO system. First, the wall clutter could be weaker, owing to the oblique angles of incidence and reflection. In essence, the transmit oblique angles in MIMO systems in conjunction with the limited-beamwidth antenna radiation patterns of the transmitter and receivers reduce the strength of the clutter compared to its counterpart in monostatic systems. Second, the propagation delay to the wall, seen from each transmit/receive antenna pair, could be different. In this case, the frequency measurements corresponding to the wall returns are no longer similar or identical, as in the case of monostatic systems. Rather, these reflections differ depending on the receiver and transmitter antenna positions. These differences deem to increase the dimension of the wall subspace, and make it difficult to distinguish from the target subspace.

In this paper, we present an extensive analysis of the SVD based wall mitigation approach under MIMO configurations. We assume the scene is stationary and

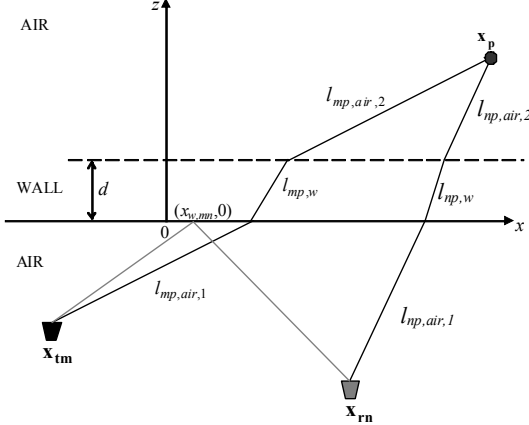


Figure 1. Geometry on transmit and receive.

change detection or Doppler processing are not applicable. We examine the wall and target subspace structures in the presence of both targets and interior walls, and contrast our findings with those under monostatic radar configuration using both simulated and experimental data.

The remainder of the paper is organized as follows. Section 2 presents the signal models for the wall and target returns under MIMO configuration. Section 3 provides the analysis of the wall and target subspaces. The subspace projection method for wall clutter mitigation under MIMO configuration is described in Section 4. Supporting simulation results are provided in Section 5 while experimental results based on real data collected in a laboratory environment are presented in Section 6. Section 7 contains the concluding remarks.

2. TWRI SIGNAL MODEL

We develop the signal model for wideband radar operation with M transmitters and N receivers. Instead of the use of orthogonal waveforms, a sequential multiplexing of the transmitters with simultaneous reception at multiple receivers is assumed. This signaling approach is a viable option for TWRI operations and is the salient feature of three known through-the-wall radar imaging systems; one is built by the Army Research Lab [8], the other by the Defense Research and Development Canada [9], and the third by MIT Lincoln Lab [4]. With the assumption of sequential multiplexing, a signal model can thus be developed based on single active transmitters.

Consider a homogeneous wall of thickness d and dielectric constant ϵ , located along the x -axis, and the region to be imaged located beyond the wall along the positive z -axis. Let the M -element transmit and the N -element receive line arrays be located parallel to the wall at standoff distances $z_{t,off}$ and $z_{r,off}$, respectively, as shown in Fig. 1. Let the m th transmitter, located at $\mathbf{x}_{tm} = (x_{tm}, -z_{t,off})$, illuminate the scene with a stepped frequency signal of K frequencies, which are equispaced over the desired bandwidth $\omega_{K-1} - \omega_0$,

$$\omega_k = \omega_0 + k\Delta\omega, \quad k = 0, 1, \dots, K-1 \quad (1)$$

where ω_0 is the lowest frequency in the desired frequency band and $\Delta\omega$ is the frequency step size. The reflections from the wall and by any targets located in the region being imaged are measured and recorded by the N -element receive array with the n th receiver location denoted by $\mathbf{x}_{rn} = (x_{rn}, -z_{r,off})$. For the case of a single point target located at $\mathbf{x}_p = (x_p, z_p)$, the output of the n th receiver corresponding to the k th frequency with the m th transmitter active is given by

$$y_m(k, n) = \sigma_w \exp(-j\omega_k \tau_{w,mn}) + \sigma_p \exp(-j\omega_k \tau_{p,mn}) \quad (2)$$

where σ_p and σ_w are the complex reflectivities of the point target and the wall, respectively, $\tau_{p,mn}$ is the propagation delay encountered by the signal as it travels from the m th transmitter to the target located at \mathbf{x}_p , and back to the n th receiver, and $\tau_{w,mn}$ is the propagation delay from the m th transmitter to the wall and back to the n th receiver. It is noted that both σ_p and σ_w are assumed to be independent of frequency and transmit and receive aspect angles. The case of frequency and aspect dependent reflectivity will be discussed in the next section. The propagation delay, $\tau_{w,mn}$, is given by

$$\tau_{w,mn} = \frac{\sqrt{(x_{tm} - x_{w,mn})^2 + z_{t,off}^2}}{c} + \frac{\sqrt{(x_{rn} - x_{w,mn})^2 + z_{r,off}^2}}{c} \quad (3)$$

where c is the speed of light in free space, and

$$x_{w,mn} = \frac{x_{tm}z_{r,off} + x_{rn}z_{t,off}}{z_{t,off} + z_{r,off}} \quad (4)$$

On the other hand, $\tau_{p,mn}$ is given by [13]

$$\tau_{p,mn} = \frac{(l_{mp,air,1} + l_{np,air,1})}{c} + \frac{(l_{mp,w} + l_{np,w})}{v} + \frac{(l_{mp,air,2} + l_{np,air,2})}{c} \quad (5)$$

where $v = c/\sqrt{\epsilon}$ is the speed though the wall, the variables $l_{mp,air,1}$, $l_{mp,w}$, and $l_{mp,air,2}$ represent the traveling distances of the signal before, through, and beyond the wall, respectively, from the m th transmitter to the target at \mathbf{x}_p , whereas $l_{np,air,1}$, $l_{np,w}$, and $l_{np,air,2}$ are the traveling distances in the air and wall from the target to the n th receiver.

In contrast, the radar return for an N -element monostatic configuration with the n th antenna located at $\mathbf{x}_n = (x_n, -z_{off})$, is given by [10]

$$y(k, n) = \sigma_w \exp(-j\omega_k \tau_w) + \sigma_p \exp(-j\omega_k \tau_{p,n}) \quad (6)$$

where $\tau_w = 2z_{off}/c$ is the two-way traveling time of the

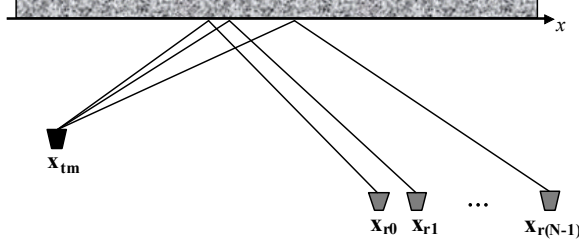


Figure 2. Wall reflections across the receive array.

signal from the n th antenna to the wall, and $\tau_{p,n}$ is the two-way traveling time between the n th antenna and the target, and is given by

$$\tau_{p,n} = \frac{2l_{np,air,1}}{c} + \frac{2l_{np,w}}{v} + \frac{2l_{np,air,2}}{c} \quad (7)$$

Unlike the MIMO configuration, the two-way signal propagation delay from each antenna to the wall surface is identical across the array aperture.

3. WALL AND TARGET SUBSPACES

With the m th transmitter active, the signals received by the N antennas at the K frequencies are arranged into an $M \times K$ matrix, \mathbf{B}_m ,

$$\mathbf{B}_m = [\mathbf{b}_{0m} \ \dots \ \mathbf{b}_{nm} \ \dots \ \mathbf{b}_{(N-1)m}], \quad (8)$$

where \mathbf{b}_{nm} is the $K \times 1$ column vector containing the stepped-frequency signal received by the n th antenna with the m th transmitter active,

$$\mathbf{b}_{nm} = [y_m(0,n) \ \dots \ y_m(k,n) \ \dots \ y_m(K-1,n)]^T. \quad (9)$$

The eigen-structure of the imaged scene is obtained by performing the SVD of \mathbf{B}_m ,

$$\mathbf{B}_m = \mathbf{U}_m \mathbf{D}_m \mathbf{V}_m^H, \quad (10)$$

where H denotes the Hermitian transpose, \mathbf{U}_m and \mathbf{V}_m are unitary matrices containing the left and right singular vectors, respectively, and \mathbf{D}_m is a diagonal matrix containing the singular values $\lambda_{1m}, \lambda_{2m}, \dots, \lambda_{Nm}$ in decreasing order, i.e., $\lambda_{1m} \geq \lambda_{2m} \geq \dots \geq \lambda_{Nm}$.

In examining (2) when the m th transmitter is active, we observe that the round-trip propagation delay encountered by the signal component reflected by the wall increases from one end to the other end of the receive array, as illustrated in Fig. 2. As a consequence, the columns of the B-scan matrix in (8) for a scene consisting of the homogeneous wall only are linearly independent, and, thus, the wall reflections corresponding to the m th transmitter span a multi-dimensional subspace. This holds true when the wall reflectivity is a function of frequency as well as transmit and receive aspect angles. On the other hand, we note from (6) that for monostatic operation with an array parallel to a homogenous wall, the wall return is independent of the antenna location,

and thus, the corresponding B-scan matrix would be of rank one, even if the wall reflectivity is frequency dependent, implying that the homogeneous wall subspace is one-dimensional for monostatic operation [6]. Comparing the target returns in (2) and (6), we observe that, similar to the monostatic operation, the target reflections under MIMO configuration span a multi-dimensional subspace whose dimensionality is affected by several factors, such as the target location, the number of targets in the scene, and the size and the geometry of the array apertures.

From the above observations, we deduce that unlike the monostatic case, it may be difficult to decouple the wall and target subspaces under MIMO configurations.

4. WALL CLUTTER MITIGATION

The problem of decoupling the wall and the target subspaces for a MIMO radar system can be resolved by preprocessing of the received data corresponding to the m th active transmitter so as to make the wall subspace appear similar to that under monostatic operation. This can be achieved as follows.

- a) Given the transmitter and receiver locations, the time delay encountered by the front wall component of the radar return corresponding to the m th active transmitter can be determined for each receiver and equalized to render the front wall return component a constant across the receive array. That is,

$$\begin{aligned} \bar{y}_m(k, n) &= \exp(j\omega_k \tau_{w,mn}) y_m(k, n) \\ &= \sigma_w + \sigma_p \exp(-j\omega_k (\tau_{p,mn} - \tau_{w,mn})) \end{aligned} \quad (11)$$

Note that for the case of frequency and aspect dependent wall reflectivity, the equalization will also reduce the dimensionality of the wall subspace provided that the wall reflectivity does not change rapidly from one antenna to the next over the frequency band of interest.

- b) The SVD of the B-scan matrix $\bar{\mathbf{B}}_m$, composed of the preprocessed data, is determined as

$$\bar{\mathbf{B}}_m = \bar{\mathbf{U}}_m \bar{\mathbf{D}}_m \bar{\mathbf{V}}_m^H \quad (12)$$

Then, the first L dominant singular vectors of the B-scan matrix composed of the preprocessed data are used to construct the wall subspace,

$$\mathbf{S}_{wall,m} = \sum_{i=1}^L \bar{\mathbf{u}}_{im} \bar{\mathbf{v}}_{im}^H. \quad (13)$$

Note that $L=1$ for frequency and aspect independent wall reflectivity. The subspace orthogonal to the wall subspace is,

$$\mathbf{S}_{wall,m}^\perp = \mathbf{I} - \mathbf{S}_{wall,m} \mathbf{S}_{wall,m}^H, \quad (14)$$

where \mathbf{I} is the identity matrix. To mitigate the wall returns, the B-scan matrix is projected on the orthogonal subspace

$$\tilde{\mathbf{B}}_m = \mathbf{S}_{wall,m}^\perp \bar{\mathbf{B}}_m. \quad (15)$$

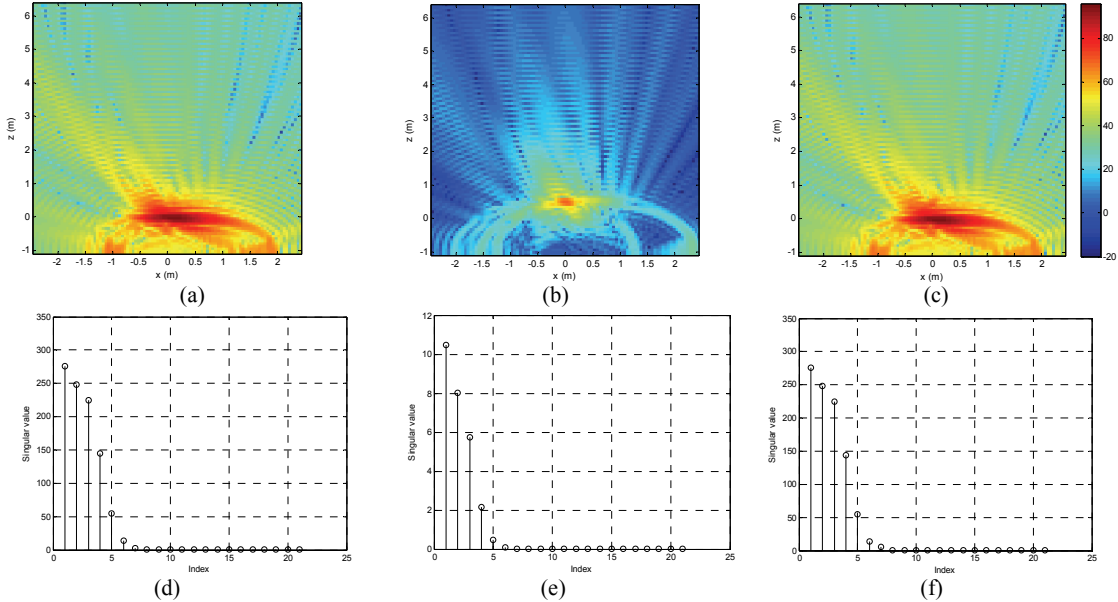


Figure 3. MIMO operation. (a) Wall only scene; (b) Target only scene; (c) Wall-plus-target scene; (d) Singular values of Wall only scene; (e) Singular values of target only scene; (f) Singular values of Wall-plus-target scene.

- c) The effect of the preprocessing on the target returns is removed from the wall-suppressed data $\tilde{y}_m(k, n)$ by applying conjugate of the equalization factor in (11). That is,

$$\hat{y}_m(k, n) = \exp(-j\omega_k \tau_{w,mn}) \tilde{y}_m(k, n) \quad (16)$$

The recovered data $\{\hat{y}_m\}_{m=0}^{M-1}$ will have little or no contribution from the wall reflections.

5. SIMULATION RESULTS

For illustration, a MIMO radar system was simulated in Matlab. The transmit and receive arrays were selected as a 5-element uniformly-spaced array of length 0.3m, centered at (-0.6, -1)m, and a 21-element uniformly-spaced array of length 1.5m, centered at (0.75, -1)m, respectively. A stepped-frequency signal covering the 1.5 to 2.5 GHz frequency band with a step size of 10 MHz was used.

First, three scenarios are considered: a homogeneous wall located along the x -axis ($z=0$), a single point target located at $(0, 0.5)$ m in free space, and the target behind the wall. The interactions between the target and the wall are ignored. The wall was chosen to be 30 dB stronger than the target, and both the target and wall reflectivities were assumed to be independent of frequency and antenna locations. Figures 3(a)-(c) illustrate the images of these three scenes and Figs. 3(d)-(f) depict their corresponding singular values with the leftmost transmitter (farthest from the receive array) active, respectively. As expected, both the target and the wall span multi-dimensional subspaces. By comparing the dominant singular values of the wall only scene with the wall plus target scene, the first five singular values are found to have similar magnitude. Figs. 4(a) and (b) show

the images of the wall only and the wall-plus-target scenes obtained after removal of the wall subspace spanned by the first five singular vectors, without any preprocessing. We observe that although most of the wall reflections are captured by the first five singular vectors, it is still difficult to locate the target using the remaining singular vectors. For comparison, Fig. 5 provides the singular values and the imaging results before and after wall mitigation for the wall-plus-target scene using a 21-element uniformly spaced monostatic array of length 1.5m at 1m standoff distance from the wall. In this case, associating the first singular value with the wall resulted in suppression of the wall returns and the target can be clearly seen. Fig. 6(a) shows the singular values of the wall-plus-target scene under MIMO configuration after preprocessing. We note that now there is only one dominant singular value. Based on a wall subspace spanned by the first singular vector, the proposed wall clutter mitigation method produces an image in which the target is clearly visible with strong reflections, as seen in Fig. 6(b).

Next, we simulated the scenario where the transmitted signal has to penetrate two consecutive walls. The MIMO configuration is now looking through two homogeneous parallel walls separated by 5m, with the target 1m behind the second wall. The received signal in this case is assumed to consist of the target return and the reflections from both walls ignoring multiple reflections between them. Both walls are assumed to have frequency and aspect independent reflectivities. Figs. 7(a) and (b) show the images before and after the proposed wall mitigation. We observe that the front wall return has been suppressed. However, the returns from the second wall are unchanged. This is because the signal traveling times from the antennas to the first wall are different from the corresponding times to the second wall. Thus, the

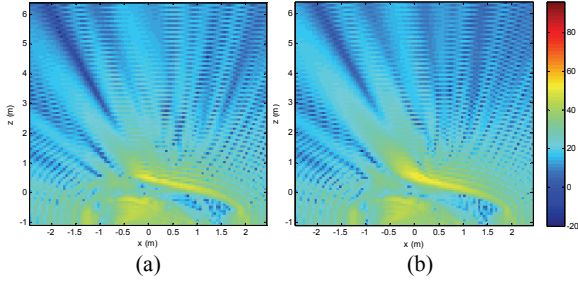


Figure 4. Reconstructed images of (a) wall only and (b) wall-plus-target scenes after removal of the wall subspace spanned by 5 singular vectors.

preprocessing only reduces the dimensionality of the first wall subspace to one. This is in contrast to the monostatic operation, where the round-trip signal traveling times from the antennas to each wall are constant across the array aperture, resulting in mitigation of both wall returns by the SVD method. This is illustrated in Figs. 7(c) and (d), which show the respective images before and after wall mitigation using the 21-element uniformly spaced monostatic array of length 1.5m at 1m standoff from the first wall.

6. EXPERIMENTAL RESULTS

A wideband MIMO TWRI system was set up in the Radar Imaging Lab at Villanova University. A stepped-frequency signal covering the 1-3 GHz frequency band with a step size of 10 MHz was chosen for imaging. An Agilent network analyzer, model ENA 5071B, was used for signal synthesis and data collection. A horn antenna, model ETS-Lindgren 3164-04, with an operational bandwidth from 0.7 to 6 GHz, was mounted on a scanner

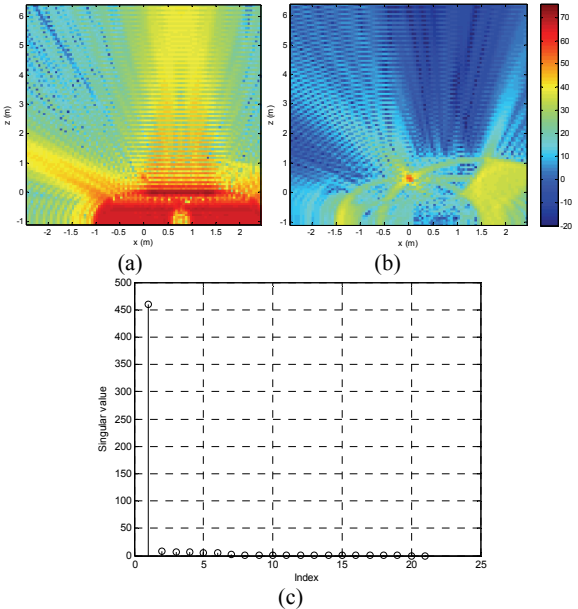


Figure 5. Monostatic radar configuration. (a)Image before wall mitigation, (b) Image after wall mitigation, and (c) Singular values of the wall-plus-target scene.

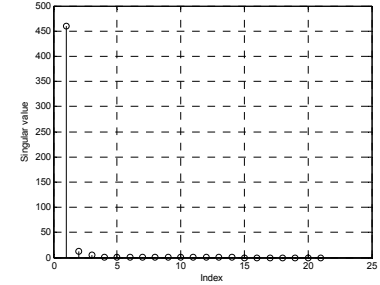


Figure 6. MIMO Results after preprocessing. (a) Wall-plus-target singular values, (b) Reconstructed image.

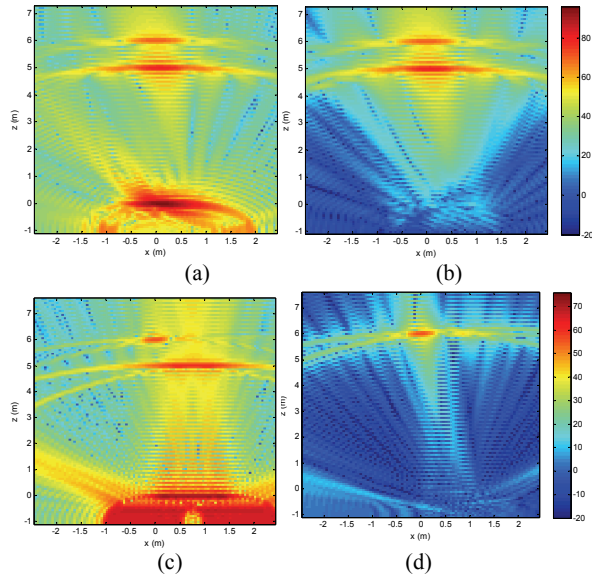


Figure 7. Two walls plus target: MIMO images (a) before, (b) after proposed wall mitigation. Monostatic images (c) before, (d) after wall mitigation.

to synthesize a uniform receive line array with an inter-element spacing of 7.49cm. Two horn antennas (model ETS-Lindgren 3164-04), mounted on tripods and placed slightly above and on either side of the receive array, were used as transmitters. A 10ft x 8ft wall segment was constructed utilizing 0.14m thick solid concrete blocks. The receive array was at a standoff distance of 1.06m from the wall, whereas the transmitters were positioned 1.34m in downrange from the wall. The experiment consisted of two humans standing at (0.51, 1.93)m and (0.11, 2.3)m in a scene populated with chairs, a desk, and a computer monitor, as shown in Fig. 8.

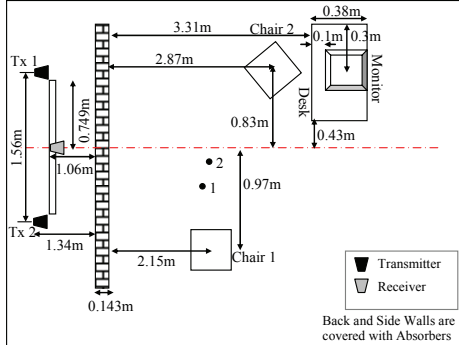


Figure 8. Scene Layout.

Figure 9(a) depicts the image obtained using the raw data. Due to the strong wall reflections, the humans cannot be seen. Figures 9(b) and (c) show the images obtained after the SVD wall mitigation with and without preprocessing, respectively, assuming that the first four singular vectors capture the wall information. Comparing the images, we see that the preprocessing step resulted in a reduced dimension subspace of the frequency and aspect dependent wall, thereby producing an image with stronger target reflections and little contribution from the wall. For comparison, the background subtracted image is provided in Fig. 9(d), which is obtained after the measurements from the empty scene with no humans were subtracted from the raw data. As background subtraction removes most of the background clutter along with the wall, the image is less cluttered than the one obtained with wall mitigation. However, the proposed method does not assume any a priori knowledge of the background scene, which is mostly unavailable in practice.

7. CONCLUSION

In this paper, we presented a detailed analysis of the subspace projection method for wall mitigation under MIMO radar configurations. The analysis showed that for a MIMO radar, both the wall and the target returns span multi-dimensional subspaces. A preprocessing step was proposed which permits decoupling of the wall and target subspaces for SVD based wall mitigation. The findings were verified using both simulated and experimental data.

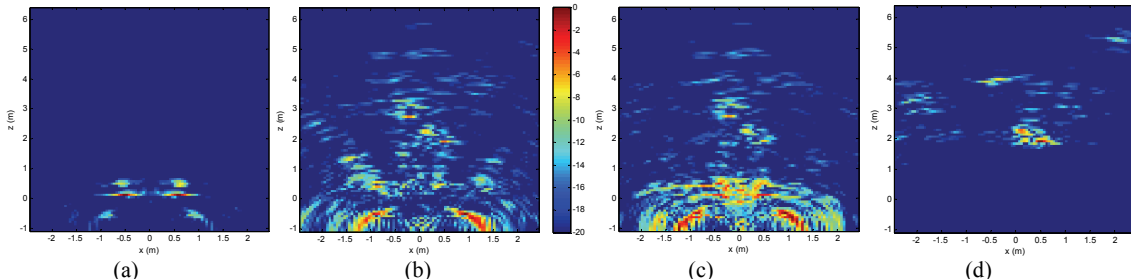


Figure 9. (a) Raw data image; (b) Reconstructed image after preprocessing; (c) Reconstructed image without preprocessing; (d) Image after background subtraction.

REFERENCES

- [1] M.G. Amin (Ed.), *Through-the-Wall Radar Imaging*, CRC Press, Boca Raton, FL, 2010.
- [2] F. Ahmad and S.A. Kassam, "Coarray analysis of the wide-band point spread function for active array imaging," *Signal Process.*, vol. 81, no. 1, pp. 99-115, Jan. 2001.
- [3] X.P. Masbernart, M.G. Amin, F. Ahmad, and C. Ioana, "An MIMO-MTI approach for through-the-wall radar imaging applications," in *Proc. 5th Int'l. Waveform Diversity and Design Conf.*, Niagara Falls, Canada, Aug. 2010, pp. 188-192.
- [4] T.S. Ralston, G.L. Charvat, and J.E. Peabody, "Real-time through-wall imaging using an ultrawideband multiple-input multiple-output (MIMO) phased array radar system," in *Proc. IEEE Int'l. Symp. Phased Array Systems and Tech.*, Boston, MA, Oct. 2010, pp. 551-558.
- [5] Y.-S. Yoon and M.G. Amin, "Spatial filtering for wall-clutter mitigation in through-the-wall radar imaging," *IEEE Trans. Geosci. Remote Sens.*, vol. 47, no. 9, pp. 3192-3208, 2009.
- [6] F.H.C. Tivive, A. Bouzerdoum, and M.G. Amin, "An SVD-based approach for mitigating wall reflections in through-the-wall radar imaging," in *Proc. IEEE Radar Conf.*, Kansas City, MO, May 23-27, 2011, pp. 519-524.
- [7] M. Dehmollaian and K. Sarabandi, "Refocusing through building walls using synthetic aperture radar," *IEEE Trans. Geosci. Remote Sens.*, vol. 46, no. 6, pp. 1589-1599, 2008.
- [8] K. Ranney et al., "Recent MTI experiments using ARL's Synchronous Impulse Reconstruction (SIRE) Radar," in *Proc. SPIE-Radar Sensor Technology XII*, April 2008, vol. 6947, pp. 694708-1-694708-9.
- [9] P. Sevigny et al., "Concept of operation and preliminary experimental results of the DRDC through-wall SAR system," *Proc. SPIE-Radar Sensor Technology XIV*, April 2010, vol. 7669, pp. 766907-1-766907-11.
- [10] F. Ahmad and M. G. Amin, "Multi-location wideband synthetic aperture imaging for urban sensing applications," *Journal of the Franklin Institute*, vol. 345, no. 6, pp. 618-639, Sep. 2008.